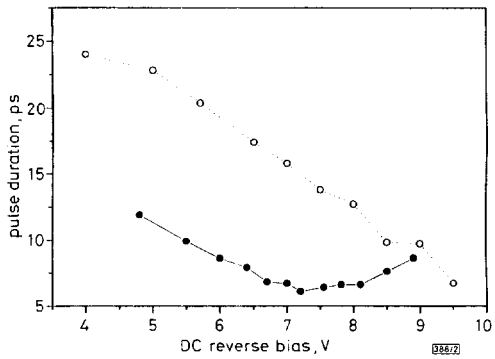

Fig. 2 *Pulse duration achieved from system at varying DC reverse bias for fixed RF drive amplitude with and without dispersion compensation*

—— compensated
····· uncompensated

spectrum correspond to the 10GHz repetition rate. The measured time-bandwidth product of these pulses was 0.32. Fig. 3*b* shows the reflection spectrum of the chirped grating measured with the broadband ASE from the preamplifier. The dip in reflectivity, which occurs in this case at 1.5622μm, was found to always be present when the grating was chirped regardless of the degree of bandwidth broadening. This dip in reflectivity is advantageous as it can help to suppress any residual CW carrier radiation transmitted by the modulator resulting in significant suppression of the background. It is believed to be due to an asymmetric temperature profile along the grating causing a slight nonlinear chirp.

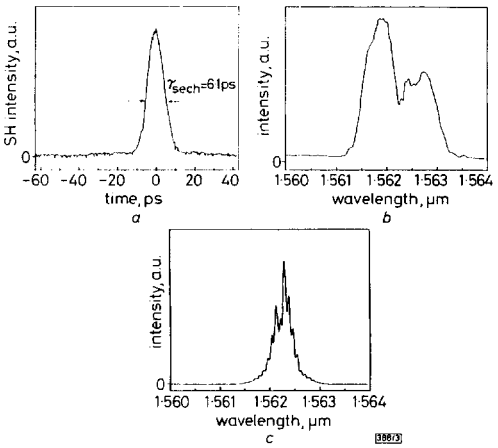

Fig. 3 *Autocorrelation trace, spectrum of pulses typically generated from the system with dispersion compensation and grating reflection spectrum with bandwidth of ~1.5nm as used in this case*

a Autocorrelation trace
b Grating reflection spectrum
c Spectrum of pulses generated from system with dispersion compensation

It should be noted that although pulses of almost comparable durations could be obtained directly from the modulator at very high DC bias values the quality of these pulses was relatively poor and they were not transform-limited. The shortest pulses generated with optimised chirp compensation were 5.2ps long and we believe this to be the shortest pulse duration obtained from an electroabsorption modulator without resort to nonlinear pulse compression techniques. We have also compressed these pulses to 180fs duration and generated pulses of tunable duration within the range 0.2–5ps using an external nonlinear compression technique. This will be reported in more detail elsewhere.

In conclusion, we have reported the use of an electroabsorption modulator in conjunction with a low insertion loss dispersive transmission filter based on a chirped fibre Bragg grating to generate high quality pulses of 5–6ps duration at 10 GHz with a duty ratio of ~6%. This method of compensating for the chirp imparted by the modulator has the advantages over the previously reported technique involving several hundreds of metres of optical fibre of being easily controllable, compact and incorporating only a few metres of fibre. In addition to dispersion correction, the fibre grating operates as a broad bandpass filter providing preamplifier noise reduction and pedestal suppression through spectral shaping. Although we produced a tunably chirped grating using a temperature gradient method to evaluate and optimise the performance of the system, the application of stable, permanent chirped gratings [7] would be preferable for practical applications.

Acknowledgments: This work was supported by the EPSRC. We would like to thank IRE POLUS GROUP for providing the diode-pumped erbium amplifiers used in the experiment.

© IEE 1995
24 February 1995
Electronics Letters Online No: 19950457

M.J. Guy, S.V. Chernikov and J.R. Taylor (*Femtosecond Group, Department of Physics, Imperial College, London SW7 2BZ, United Kingdom*)

D.G. Moodie and R. Kashyap (*BT Laboratories, Martlesham Heath, Ipswich, IP5 7RE, United Kingdom*)

References

1 WAKITA, K., SATO, K., YAMAMOTO, M., and ASOBE, M.: 'Transform-limited 7 ps pulse generation using a sinusoidally driven InGaAsP/InGaAsP strained multiple quantum well DFB laser/modulator monolithically integrated light source', *IEEE Photonics Technol. Lett.*, 1993, **5**, pp. 899–901

2 MOODIE, D.G., ELLIS, A.D., and FORD, C.W.: 'Generation of 6.3ps optical pulses at 10GHz repetition rate using a packaged electroabsorption modulator and dispersion compensating fibre', *Electron. Lett.*, 1994, **30**, pp. 1700–1701

3 OUELLETTE, F.: 'All-fibre filter for efficient dispersion compensation', *Opt. Lett.*, 1991, **16**, pp. 303–305

4 KASHYAP, R., CHERNIKOV, S.V., MCKEE, P.F., and TAYLOR, J.R.: '30 ps chromatic dispersion compensation of 400fs pulses at 100Gbit/s in optical fibres using an all-fibre photoinduced chirped reflection grating', *Electron. Lett.*, 1994, **30**, pp. 1078–1080

5 GUY, M.J., CHERNIKOV, S.V., TAYLOR, J.R., and KASHYAP, R.: 'Low-loss fibre Bragg grating transmission filter based on a fibre polarisation splitter', *Electron. Lett.*, 1994, **30**, pp. 1512–1513

6 LAUZON, J., THIBAULT, S., MARTIN, J., and OUELLETTE, F.: 'Implementation and characterisation of fibre Bragg gratings linearly chirped by a temperature gradient', *Opt. Lett.*, 1994, **19**, pp. 2027–2029

7 KASHYAP, R., MCKEE, P.F., CAMPBELL, R.J., and WILLIAMS, D.L.: 'A novel method of producing all-fibre photoinduced chirped gratings', *Electron. Lett.*, 1994, **30**, pp. 996–997

Tunable photodetectors and light-emitting diodes for wavelength division multiplexing

S. Strite and M.S. Ünlü

Indexing terms: Light emitting diodes, Photodetectors, Wavelength division multiplexing, Micromachining

The authors propose and analyse a hybrid device structure which extends the dynamic tuning range of vertical-cavity photodiodes and emitters. The device consists of a conventional, epitaxial *pin* junction quantum-well diode grown on a quarter-wave mirror stack. The upper mirror is attached to the underside of a micromachined membrane fabricated on top of the epilayer. This configuration allows the upper mirror to be electrostatically deflected towards the episurface, reducing the overall vertical cavity length which tunes the resonance wavelength over the entire free spectral range of the cavity. Simulations of the device indicate that eight-channel operation between 900 and 1000nm can be achieved with low crosstalk. It is expected that this device will find use in wavelength-division-multiplexing applications.

Introduction: The bandwidth of optical communication networks can be improved by either increasing device speeds or by more fully utilising the fibre bandwidth via wavelength division multiplexing (WDM). Vertical cavity (VC) structures [1] are favourites for both approaches due to improved photodiode (PD) detector bandwidth [2, 3], the ability to change the resonance wavelengths of both PDs and emitters by physically varying the optical length of the VC [4, 5], and their potential for integration due to the similarity of VC emitter and PD *pin* structures [6, 7]. An ideal device for WDM applications must be dynamically tunable with a flat response across a maximum wavelength range while being subjected to minimal interchannel crosstalk. However, many schemes proposed to date are either not dynamically tunable [6, 7] or cannot be tuned over a sufficiently wide wavelength range [8, 9] to be useful for WDM applications. In the past couple of years, advances in micromachining have permitted researchers to demonstrate several schemes in which a Fabry-Perot (FP) microcavity is modulated by a physically movable mirror [10 – 13], granting access to a large-wavelength tuning mechanism on the microsecond timescale.

Here we propose and analyse a new extended vertical cavity (EVC) device in which an Au top mirror is attached to the underside of a micromachined SiN_x membrane fabricated on top of an epitaxial VC LED or PD structure. Electrostatic deflection of the membrane displaces the mirror towards the episurface, decreasing the overall cavity length, thereby tuning the VC resonance emission or detection wavelength [10, 13]. The nature of VCs should permit high-yield, low-cost VC LEDs and PDs to be fabricated which permit reproducible tuning of a narrow active wavelength band across 100nm on a microsecond timescale. Implementations of the EVC scheme which should find wide application in WDM networks are described.

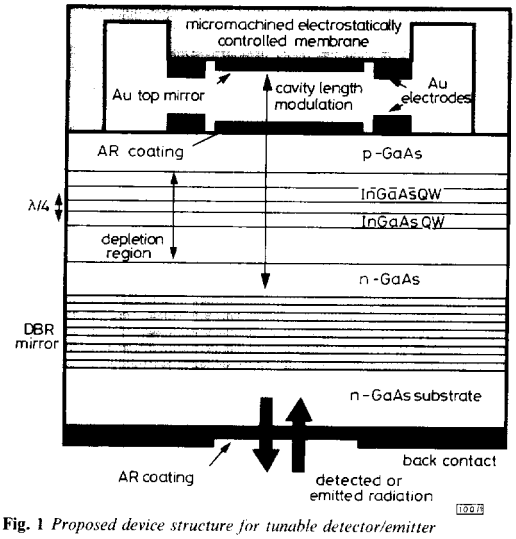

Fig. 1 *Proposed device structure for tunable detector/emitter*

Device structure and method: Fig. 1 is a schematic diagram of the proposed tunable EVC LED/PD structure realised in the InAlGaAs material system. The concepts described below remain equally valid for other material systems optimised for different wavelengths, although the performance may vary. The structure is essentially a conventional VC device [1] in which the top mirror is positioned on the underside of a micromachined membrane as opposed to the episurface. The EVC is defined by the lower AlAs/GaAs DBR and the upper Au mirror, and contains two strained InGaAs quantum-well (QW) active regions surrounded by GaAs spacer layers. Only the InGaAs QW active regions have significant absorption coefficients in the 900 1000nm wavelength region of interest.

The quarter-wavelength separation between the two QWs suppresses variations in the device performance which would otherwise result from the shifting electric field standing-wave distribution in the cavity during tuning. The asymmetric positioning of the QWs within the spacer layers equalises the electron and hole transit times to/from the contacts, significantly increasing the device bandwidth [2]. The antireflection (AR) coating between the episurface and the upper Au mirror minimises stray reflections within the airgap, flattening the device response across the tuning range. The AR coating on the GaAs substrate back is critical to the external efficiency in ensuring efficient coupling of radiation into or out of the device. The resonance frequency of the EVC is tuned when electrostatic downward deflection of the membrane decreases the total cavity length [10, 13].

The epitaxial structure can be grown and fabricated by conventional semiconductor epitaxial and processing techniques. The above design should permit high yield because the cavity response can be pretuned after the epitaxial growth by etching back some of the surface material before the deposition of the AR coating and membrane mirror [4, 14]. By fine-tuning the epitaxial structure after growth, an essentially identical initial VC can be consistently provided to the fabrication process.

The SiN_x membrane and Au mirror can be fabricated by increasingly conventional micromachining techniques at low temperatures so that the active device structure is not degraded. Care must be taken in the membrane design to avoid mirror bowing during both fabrication and operation which would lead to a rapid degradation of the cavity finesse. To that end it is sensible to design thin flexible arms for the membrane so that the bowing occurs there.

Simulation results and discussion: The EVC was modelled using a transmission-line model [15] in which the wavelength-dependent impedance is calculated at every interface [16]. The values for the wavelength-dependent absorption coefficients and refractive indices have been tabulated and are readily available [17].

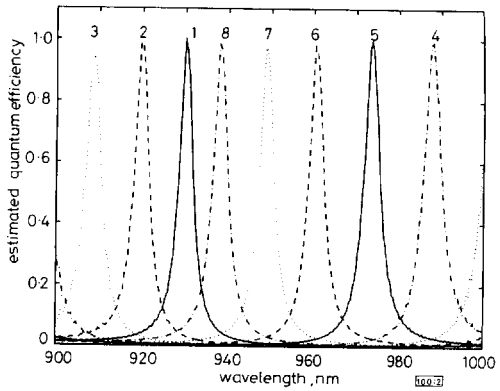

Fig. 2 *Spectral response of EVC device optimised for eight-channel operation between 900 and 1000nm*

Trace 1 corresponds to undeflected membrane. Successive traces represent 60nm deflection steps. Spectrum repeats itself beyond eighth trace ($\lambda/2$ total mirror displacement)

Fig. 2 shows the calculated spectral response of the EVC device of Fig. 1 as a function of the Au top mirror displacement. The device is optimised for eight-channel operation between 900 and 1000nm. In PD (LED) mode, the y-axis represents the generated photocurrent (output power) in arbitrary units, respectively. The VC dictates the narrow response spectra by either rejecting incoming light (PD) [4] or by inhibiting spontaneous emission (LED) [18] at off-resonance wavelengths. Furthermore, the VC effect is known to increase the sensitivity of PDs significantly [4], and the spectral power density and directivity of LEDs [18], so that each device has superior performance compared to its conventional counterpart. The total number of channels is limited by the stopband width of the bottom DBR mirror, which results in decreased efficiencies at wavelengths outside the 900–1000nm band. An optimised bottom AR coating is critical for preventing the formation of an additional VC between the DBR and substrate back whose spectrum would superimpose itself onto the response of the main cavity, degrading the device performance.

An 11-period GaAs/AlAs bottom DBR mirror enables the structure to function with a crosstalk of ~1:40. Similar calculations on a InGaAlAs structure lattice-matched to InP for 1500–1600nm operation required a 22-period DBR to attain a crosstalk of ~1:8. This result is solely attributable to the smaller refractive index contrast between InGaAs and InAlAs.

The basic EVC device structure incorporates several advantages which should make it a powerful and cost-effective component for short-haul communication systems. The wavelength selectivity of the VC dictates a narrow response suitable for WDM applications. Furthermore, the VC implementations of both LEDs and PDs offer drastically improved performance compared to their conventional counterparts which would significantly increase the capabilities of systems incorporating them. For example, VC LEDs [18] have zero threshold current, negligible temperature/wavelength dependence and high directivity for improved fibre coupling. Vertical vavity PDs [1, 2] have a significantly improved bandwidth compared to conventional structures and a near-unity quantum efficiency at resonance. The high quantum efficiency of the PDs further mitigates the need for expensive laser sources.

Fabrication of EVC devices should be simpler than VC lasers due to the less stringent cavity requirements. The hybrid top mirror design provides both a higher Q cavity than simpler designs [13] and a pretuning capability before the membrane evaporation to increase epitaxial yield. Flexible membrane devices can be operated at Mbit/s switching rates [11, 13], proving their practicality for WDM systems. These combined functions make EVC devices highly attractive as inexpensive, yet powerful, emitter/detector elements for WDM local-area networks.

Acknowledgments: This research is supported by the National Science Foundation under grant ECS-9309607.

© IEE 1995
30 January 1995
Electronics Letters Online No: 19950452

S. Strite (*IBM Research Division, Zurich Research Laboratory, 8803 Rüschlikon, Switzerland*)

M.S. Ünlü (*Boston University, Center for Photonics Research and Department of Electrical, Computer and Systems Engineering, 44 Cummington Street, Boston, MA 02215, USA*)

References

1 ÜNLÜ, M.S., and STRITE, S.: 'Resonant cavity enhanced (RCE) photonic device', *J. Appl. Phys. Rev.*, in press

2 ÜNLÜ, M.S., LEBLEBICI, Y., KANG, S.M., and MORKOÇ, H.: 'Transient simulation of resonant cavity enhanced heterojunction photodiodes', *IEEE Photonics Technol. Lett.*, 1992, **4**, pp. 1366–1369

3 PRANK, U., and KOWALSKY, W.: 'Wavelength selective metal-semiconductor-metal photodetector with integrated Fabry-Perot resonator for high bandwidth receivers', *Jpn. J. Appl. Phys.*, 1993, **32**, p. 574

4 ÜNLÜ, M.S., KISHINO, K., CHYI, J.-I., REED, J., ARSENAULT, L., and MORKOÇ, H.: 'Wavelength demultiplexing heterojunction phototransistor', *Electron. Lett.*, 1990, **26**, pp. 1857–1858

5 CHANG-HASNAIN, C.J., HARBISON, J.P., ZAH, C.E., MAEDA, M.W., FLOREZ, L.T., STOFFEL, N.G., and LEE, T.P.: 'Multiple wavelength tunable surface emitting laser arrays', *IEEE J. Quantum Electron.*, 1991, **27**, pp. 1368–1376

6 ÜNLÜ, M.S., STRITE, S., DEMIREL, A.L., TASIRAN, S., SALVADOR, A., and MORKOÇ, H.: 'Wavelength selective optical logic and interconnects', *IEEE J. Quantum Electron.*, 1993, **29**, pp. 411–425

7 ZHOU, P., CHENG, J., SCHAUS, C., SUN, S., HAINS, C., ARMOUR, E., MYERS, D., and VAWTER, G.: 'Inverting and latching optical logic gates based on the integration of vertical-cavity surface-emitting lasers and photothyristors', *IEEE Photonics Technol. Lett.*, 1992, **4**, pp. 157–159

8 WIPIEJEWSKI, T., PANZLAFF, K., and EBELING, K.J.: 'Tunable extremely low threshold vertical-cavity laser diodes', *IEEE Photonics Technol. Lett.*, 1993, **5**, pp. 889–892

9 LAI, K., and CAMPBELL, J.C.: 'Design of a tunable GaAs/AlGaAs multiple-quantum-well resonant cavity photodetector', *IEEE J. Quantum Electron.*, 1994, **30**, pp. 108–114

10 PEZESHKI, B., and HARRIS, J.: 'Electrostatically tunable optical device device and interconnect for processors'. US Patent #5291502

11 ARATANI, K., FRENCH, P.J., SARRO, P.M., POENAR, D., WOLFFENBUTTEL, R.F., and MIDDELHOEK, S.: 'Surface micromachined tunable interferometer array', *Sens. Actuators*, 1994, **A-43**, pp. 17–23

12 JAECKLIN, V.P., LINDER, C., BRUGGER, J., DE ROOIJ, N.F., MORET, J.-M., and VUILLEUMIER, R.: 'Mechanical and optical properties of surface micromachined torsional mirrors in silicon, polysilicon and aluminium', *Sens. Actuators*, 1994, **A-43**, pp. 269–275

13 GOOSSEN, K.W., WALKER, J.A., and ARNEY, S.C.: 'Silicon modulator based on mechanicallly-active anti-reflection layer with 1 Mbit/sec capability for fiber-in-the-loop applications', *IEEE Photonics Technol. Lett.*, 1994, **6**, pp. 1119–1121

14 KARIM, Z., KYRIAKAKIS, C., TANGUAY, Jr., A.R., HU, K., CHEN, L., and MADHUKAR, A.: 'Externally deposited phase-compensating dielectric mirrors for asymmetric Fabry-Perot cavity tuning', *Appl. Phys. Lett.*, 1994, **64**, pp. 2913–2915

15 HAUS, H.: 'Waves and fields in optoelectronics' (Prentice Hall, London, 1984), pp. 41–46

16 CHENG, D.K.: 'Field and wave electromagnetics' (Addison Wesley Publishing Co., New York, 1989), pp, 368–369, 451

17 MADELUNG, O. (Ed.): 'Physics of group IV and II–V compounds', Landolt-Börnstein new series vol. III/17a (Springer Verlag, New York, 1982)

18 SCHUBERT, E.F., HUNT, N.E.J., MICOVIC, M., MALIK, R.J., SIVKO, D.L., CHO, A.Y., and ZYDIK, G.J.: *Science*, 1994, **265**, p. 943

Seasonal propagation effects in an obstructed rural radio path at 462MHz

N. Evans

Indexing terms: Radiotelemetry, Radiowave propagation

The Letter reports on a 12month observation of signal strength in a 462MHz radio link operating over a 2.4km, irregular rural path containing a deciduous tree grove 150m in diameter. The received signal level was biphasic, with temporal changes of 1.8 and 6.7dB/month at the beginning and end of foliation, respectively. There was a maximum shift of 8dB from summer to winter and up to 2dB variation from wet to dry conditions.

Introduction: Short radio paths are used in rural areas for animal telemetry and for agricultural purposes. Remote transmitters/receivers are necessarily compact, battery powered and operate to a strict power budget; output signal/noise ratios may be marginal, and the reliability of uncoded digital links will deteriorate seriously with relatively small increases (3–5dB) in path loss [1]. Antennas are near ground level in many telemetry and telecommand applications, so paths are liable to suffer significant excess loss due to obstructing hills and vegetation. Distraction loss and the loss due to wooded regions may be calculated with reasonable accuracy, but changes due to leaf generation and subsequent depletion require experimental measurement. Although some workers have sampled path loss in selected wooded regions under no-leaf and full-leaf conditions, little information is available on full seasonal changes.

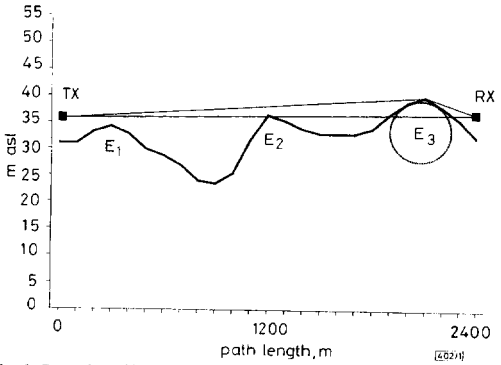

Fig. 1 *Ground profile of short rural path investigated*

Experimental work: A 12 month monitoring exercise was carried out on a 462MHz link between two fixed stations, operating over